ACS APPLIED MATERIALS & INTERFACES

Research Article

Cite This: ACS Appl. Mater. Interfaces 2017, 9, 38323-38335

www.acsami.org

Self-Powered Nanocomposites under an External Rotating Magnetic Field for Noninvasive External Power Supply Electrical Stimulation

Fengluan Wu, Long Jin, Xiaotong Zheng,* Bingyun Yan, Pandeng Tang, Huikai Yang, Weili Deng, and Weiqing Yang*

School of Materials Science and Engineering, Key Laboratory of Advanced Technologies of Materials, Ministry of Education, Southwest Jiaotong University, Chengdu 610031, China

Supporting Information

ABSTRACT: Electrical stimulation in biology and gene expression has attracted considerable attention in recent years. However, it is inconvenient that the electric stimulation needs to be supplied an implanted power-transported wire connecting the external power supply. Here, we fabricated a self-powered composite nanofiber (CNF) and developed an electric generating system to realize electrical stimulation based on the electromagnetic induction effect under an external rotating magnetic field. The self-powered CNFs generating an electric signal consist of modified MWNTs (m-MWNTs) coated Fe_3O_4/PCL fibers. Moreover, the output current of the nanocomposites can be increased due to the presence of the magnetic nanoparticles during an external magnetic field is applied. In this paper, these CNFs were employed to replace a bullfrog's sciatic nerve and to realize the effective functional electrical stimulation. The cytotoxicity assays and animal tests of the nanocomposites were also used to evaluate the biocompatibility and tissue integration. These results demonstrated that this self-powered CNF not only plays a role as power source but also can act as an external power supply under an external rotating magnetic field for noninvasive the replacement of injured nerve.

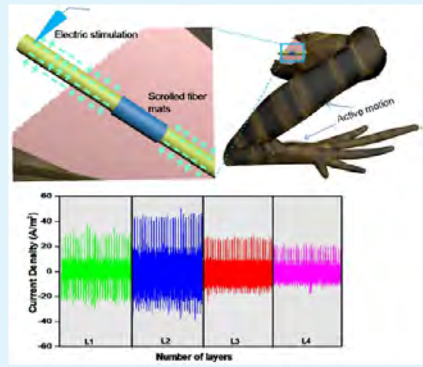

KEYWORDS: *self-powered, nanofibers, noninvasive, external magnetic field, electromagnetic*

1. INTRODUCTION

Electric stimulation has widely been used in biological and medical applications, including functional electrical stimulation, neurite outgrowth, and cerebral cortex. Exogenous electrical stimulation has been effectively used in both clinical practice and laboratory research to stimulate neurite outgrowth,[1,2] regulate differentiation[3,4] and cerebral cortex,[5] heal injured skin,[6] establish a regeneration model of specific tissues in the stump of a rat limb amputation,[7] and promote cardiomyocyte maturation.[8] In addition, a variety of conductive materials have been used in electrical stimulation,[9−11] Huang et al. developed a CNT ropelike substrate that was allowed to generate electrical stimulation in order to promote the extension of neurite outgrowth in the early culture stage.[9] Vitale et al. demonstrated neural recording and stimulation with soft CNT fiber microelectrodes.[10] Min et al. have described sulfonated polyaniline based organic electrodes to control electrical stimulation.[11]

However, the connecting requirement of an external power source to enable the electrical stimulation process is inconvenient in biomedical applications because of the use of bioelectrodes, chips, cell-membranes and a conductive polymer platform as the internal−external conducting medium.[12−17] Developing a wireless power source supply with simple electronic transport remains a challenge, especially for electrical stimulation.[18−21] Inspired by wearable electronics that harvest solar and mechanical energy for self-powered system, we designed a noninvasive external power supply and self-powered composites.[22−30]

In this paper, we demonstrated a facile method to fabricated a noninvasive external power supply using a self-powered self-powered composite nanofiber (CNF) composed of m-MWNTs coated Fe_3O_4/PCL nanofibers under an external alternating magnetic field.[31−34] On the basis of the electromagnetic induction effect, this self-powered nanocomposite can generate power when an external magnetic field is applied to the CNF. At the same time, the CNF can freely control the on/off self-powered motion when the designed magnetic field stops rotating. For the first time, we fabricated a directional wire comprising m-MWNTs coated on the matrix of Fe_3O_4/PCL electrospinning nanofibers.

This nerve-like network wire imitates the structure of nerve fibers, which have an excellent conductivity. For instance, this CNF can effectively produce electricity by applying an external magnetic field, thereby representing its potential to realize electrical stimulation by acting as a noninvasive external power supply. Moreover, we examined the biological applications of the CNFs by replacing a bullfrog's sciatic nerve to realize

Received: August 25, 2017
Accepted: October 17, 2017
Published: October 17, 2017

DOI: 10.1021/acsami.7b12854
ACS Appl. Mater. Interfaces 2017, 9, 38323−38335

functional electrical stimulation, as well as evaluating its cytotoxicity and testing its tissue integration using a rabbit muscle implantation test.

2. EXPERIMENTAL SECTION

2.1. Materials. Raw PCL with a weight-average molecular weight (M_w) of 112 kDa was synthesized as described in a previous report.[35] MWNTs with an outer diameter of 20−30 nm and a length of 10−20 μm, synthesized by chemical vapor deposition, were purchased from Chengdu Institute of Organic Chemistry, Chinese Academy of Sciences. Dichloroethane (DCE), *N*,*N*-dimethylformamide (DMF), and ethanol were purchased from Chengdu Kelong Chemical Reagent Factory. Deionized (DI) water was used in all experiments. All other chemicals and solvents were of reagent grade or better and were used without further purification.

2.2. Fabrication of Fe_3O_4/PCL Nanofibers. Superparamagnetic iron oxide nanoparticles (SPIONs) were prepared by chemical codeposition and modified by oleic acid similar to the previous reports.[36,37] First, 4.1 g of $FeCl_3·6H_2O$ was added to 100 mL of distilled water at 50 °C with mechanically stirring under N_2 protection. Second, 1.79 g of $FeCl_2·4H_2O$ was dissolved into the solution, then 20 mL of $NH_3·H_2O$ added, and the temperature increased 80 °C. Next, oleic acid was also added into the resulting solution under strong stirring. The resultant Fe_3O_4 nanoparticles were washed and then kept in dimethylbenzene solution. These nanoparticles were well-dispersed in a mixed solution of methylene chloride and DMF, and PCL was dissolved in the mixture. After mechanically stirring overnight, the mixture was poured into a 5 mL syringe connected to a hollow metal capillary with a 1.5 m polyethylene catheter. The nanofiber mats were prepared with different Fe_3O_4/PCL ratios (w/w: 0, 0.2, 0.4, 0.6, 0.8, 1.0, 1.2, and 1.4%).

A power supply was used to provide a potential of 21 ± 0.5 kV, and the polymer solution flow was controlled at a constant flow rate of 0.8 mL/h. The aligned nanofiber mats were prepared and collected by a drum wrapped with aluminum foil at 1000 rpm. The distance between needle and receiver was 15 cm. All experimental procedures were carried out at room temperature, and the mats were dried under vacuum at room temperature.

2.3. Fabrication of m-MWNT Coated Fe_3O_4/PCL Fiber Mat Nanocomposites. The fabrication of the conductive m-MWNT coated Fe_3O_4/PCL nanofiber nanocomposites could be accomplished by the following steps: Raw MWNTs were acid oxidized similar to a previous report.[38,39] Briefly, the raw MWNTs was added to hydrochloric acid (HCl) under stirring for 2 h at room temperature and, then were diluted by water, filtered, washed with deionized water, and dried under vacuum at 40 °C overnight. Next, the pretreated MWNTs were added to nitric acid (HNO_3), heated at 140 °C for 4 h, and then cooled to room temperature. Finally, the procedures described above were repeated once more.

To prepare a 5 mg/mL m-MWNT suspension, m-MWNTs were dispersed in absolute ethanol with ultrasonication for 1 h, and then half of them were added to a certain proportion of methylene chloride. To fabricate the conductive nanocomposites, the m-MWNTs were coated onto the matrix of the Fe_3O_4/PCL nanofiber mats using a vacuum-assisted spray technique at a rate of 0.6 mL·s^{-1}.[40,41] Hence, the cumulative weight of m-MWNTs would be expressed as the weight per unit area of composite mat.

2.4. Electromagnetic Induction Effect under External Magnetic Field. To realize the electromagnetic induction effect, an external rotating magnetic field was self-built. Different rotation speeds of the lab-built rotating magnetic field could be achievzed by changing the rotation speed and were controlled by an ammeter (Stanford Research RS570).

The calculation of the power density and the resistivity was performed as follows. The power density of the CNFs under an external magnetic field can be expressed as

$$C_d = I/S$$

The resistivity of CNFs can be expressed as

$$\rho = RS/L$$

where C_d is the current density, I is the short-circuit current, S is the cross-sectional area, ρ is the resistivity, and L is the length of the CNFs.

2.5. *In Vitro* Cytotoxicity Assays. The cytotoxicity assay was carried out on endothelial cells (ECs) based on an Alamar Blue assay, as described previously.[42] Cells were seeded into 24-well plates with a density of 2 × 10^4 cells/well. CNF samples were sterilized for 4 h by UV radiation with a power of 100 W. CNFs with different amounts of m-MWNTs were cut into small round flakes with average diameters of nearly 10 mm, and the CNF samples were immersed in the culture medium and fixed between two rings. The culture medium was refreshed every 2 days. On days 1, 3, 5, and 7, an Alamar Blue assay was performed, and the absorbance of Alamar Blue solution was read using an ELISA microplate reader (Molecular Devices, Sunnyvale, CA) after 4 h of incubation at 570 nm. Meanwhile, the cells were stained with 1 μM calcein AM and propidium iodide (PI) (Sigma, USA) and then observed by fluorescence microscopy (CKX 41, Olympus, Japan) at each point. The ECs were cultured in F12 medium supplemented with 10% fetal bovine serum (FBS) and maintained at 37 °C and 5% CO_2 under fully humidified conditions.

2.6. Animals. *2.6.1. Functional Electrical Stimulation.* Bullfrog (75 ± 5 g) sciatic nerves were used for functional electrical stimulation. The bullfrogs were purchased from local famers.

To establish a sciatic nerve defect model, a bullfrog was sacrificed. First, a hind limb of the bullfrog was chosen and kept in Ringer's solution. Second, the hind limb was dissected, the sciatic nerve exposed, and the empty defect replaced by CNFs with 0.259 mg/cm^2 m-MWNTs (8 × 10 mm, diameter × length). Animal experiments were carried out in compliance with the guidelines and approved by the Institutional Animal Care.

2.6.2. Tissue Integration. The biocompatiblity of CNFs for muscle tissue integration were demonstrated by *in vivo* implantation. CNFs with different amounts of m-MWNTs (8 × 10 mm, diameter × length) were implanted into the hind leg muscle of a rabbit model to evaluate its tissue integration. All samples were sterilized for 4 h by UV radiation with a power of 100 W.

2.6.3. Surgery. In brief, the two male New Zealand white rabbits weighing 2.5 ± 0.02 kg used as the *in vivo* muscle model were purchased from the Experimental Animal Center of Sichuan Province and raised for 2 weeks before surgery. After being anesthetized with pentobarbital (2 wt %, 30 mg/kg) and lidocaine (2 wt %), the rabbits were implanted with the prepared sample. The rabbits were housed and injected with penicillin (80 units/ml) on day 3 following the surgery. The animals were kept in two cages. All animal procedures were performed in accordance with the protocols approved by the local Ethical Committee and followed the Laboratory Animal Administration Rules of China.

During the treatment period, the rabbits showed no adverse reaction and no inflammation. At 4 weeks postsurgery, the rabbits were sacrificed, and samples were harvested for further examination. Photographs of the surgical procedure were taken by a digital camera.

2.6.4. Histological Examination. At 4 weeks postsurgery, the tissues implanted with the CNFs were collected in a solution of formaldehyde, glacial acetic acid, and absolute ethanol and embedded in paraffin blocks. Then, the tissue sections were stained with hematoxylin/eosin (H&E) for microscopic observation.

2.7. Characterization. *2.7.1. Fourier Transform Infrared Spectroscopy.* Fourier transform infrared spectroscopy (FTIR; Nicolet 5700) was performed to analyze the surface modification of the MWNTs, Fe_3O_4 nanoparticles and m-MWNT coated Fe_3O_4/PCL fiber mats. These specimens of the m-MWNTs and magnetic nanoparticles were made into powder and mixed with KBr at a weight ratio of 0.5−1%.

2.7.2. Field-Emission Scanning Electron Microscopy. The morphology of the electrospun Fe_3O_4/PCL fiber mats and m-MWNT coated Fe_3O_4/PCL mats were characterized using a JSM-7001F field-emission scanning electron microscope (FE-SEM, JEOL,

DOI: 10.1021/acsami.7b12854
ACS Appl. Mater. Interfaces 2017, 9, 38323−38335

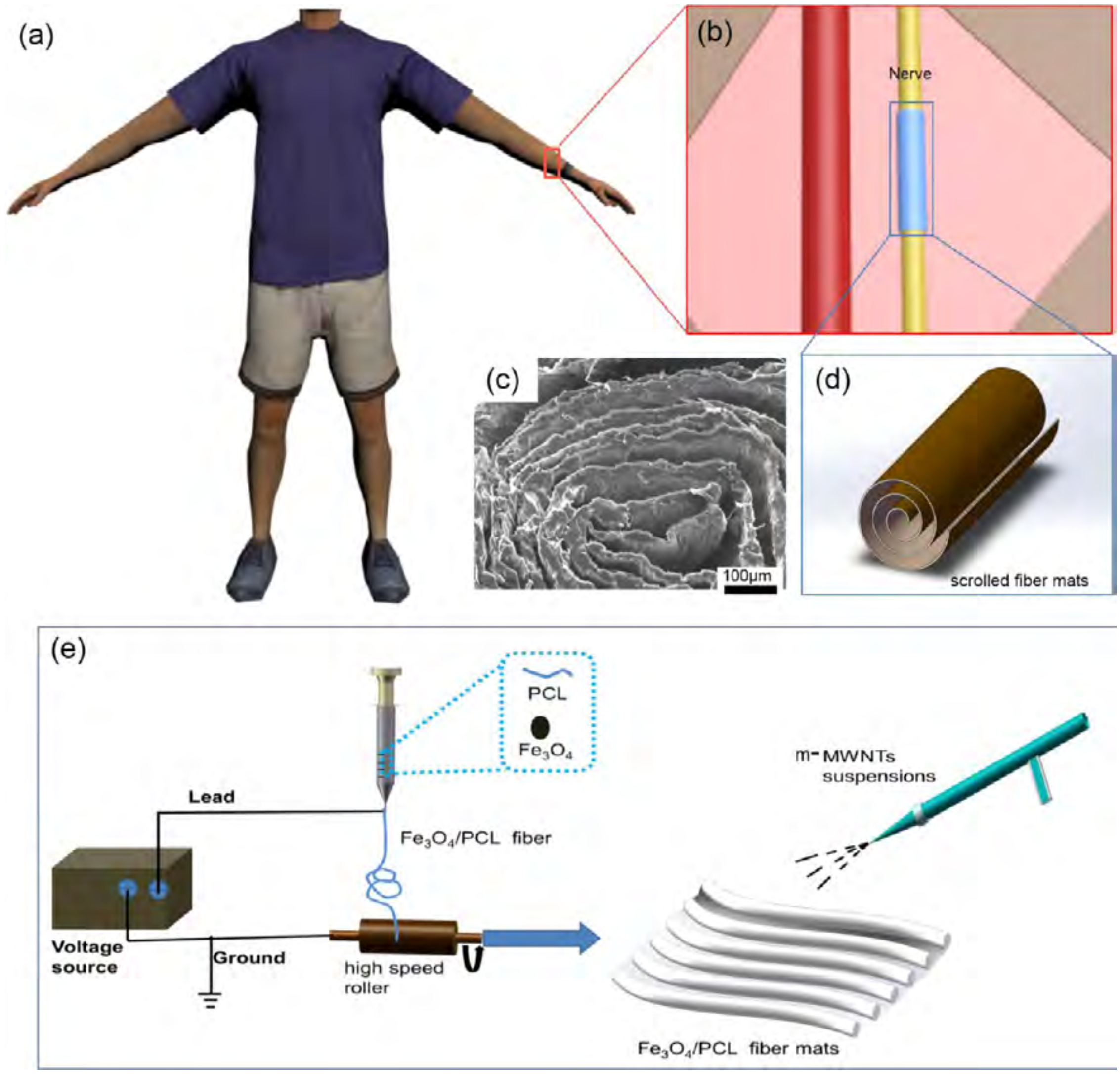

Figure 1. Structural design of scrolled fiber mats self-powered by an external magnetic field and the use of these mats to replace an injured nerve. (a, b) Schematic illustrations of a human (a) and the human's nerves (b). (c) Schematic models of Fe_3O_4/PCL fiber mats coated with MWNTs. (d) Cross-sectional SEM image of the surface of the scrolled fiber mats. (e) Schematic illustration of the fabrication of electrospinning ordered Fe_3O_4/PCL fiber composites coated with m-MWNTs.

Japan). The Fe_3O_4/PCL fiber mats were sputter coated with gold to observe their surface topographies.

2.7.3. Field-Emission Transmission Electron Microscopy. The microstructures of the nanofibers, the alignment and dispersion of the Fe_3O_4 nanoparticles and the m-MWNT coated Fe_3O_4/PCL nanofiber mats were observed by a field-emission transmission election microscope (FE-TEM, JEM-2100F, JEOL, Japan) operating at 200 kV.

2.7.4. Vibrating Sample Magnetometer. The magnetic properties of the Fe_3O_4/PCL fiber mats were measured with a vibrating sample magnetometer (VSM, Lake Shore 7410, America) under the conditions of 300 K, 1000 Am^{-1}, and 16 Hz.

2.7.5. Current Signal Characterization of the Samples. The output current signals of all samples were measured by a low-noise current preamplifier (Stanford Research RS570). The resistance of all samples was measured by a Keithley 6514 system.

3. RESULTS AND DISCUSSION

3.1. Design and Characterization of Self-Powered Nanocomposites under an External Rotating Magnetic Field. We were inspired by the concept of self-powered nanocomposites and wireless power supply and by the reports of magnetic nanomotors powered by a rotating magnetic field and electrical stimulation provided by a nanogenerator published by Zhu et al. and Rui et al., respectively.[12,22−31] Accordingly, we have designed a novel conductive nanomaterial consisting of m-MWNT coated Fe_3O_4/PCL fiber mats and aimed to realize noninvasive electrical stimulation using an external power supply. Electrospun polymer nanofibers have recently attract interest for biological applications. Here, our fabrication method consists of (i) the dispersion of m-MWNTs in a mixed solution (ethanol and DCE), (ii) the preparation of Fe_3O_4/PCL/DCE/DMF solution, and (iii) the incorporation of the m-MWNTs by spraying the solution from (i). The m-MWNTs were embedded in the Fe_3O_4/PCL matrix, and the morphological interactions between the composites and the degree of anchoring of the m-MWNTs on the surfaces were dependent on the hydrophilicity/hydrophobicity of the species, the absorption of the m-MWNT surfaces, the mixed solution (DCE and DMF), the carboxyl groups on Fe_3O_4 and those on the m-MWNTs forming hydrogen bonds, and the adhesion of the m-MWNTs after acid treatment.[43−45]

Figure 1a−c displays the use of the scrolled fiber mats to replace an injured nerve. A cross-sectional FE-SEM image of

DOI: 10.1021/acsami.7b12854
ACS Appl. Mater. Interfaces 2017, 9, 38323−38335

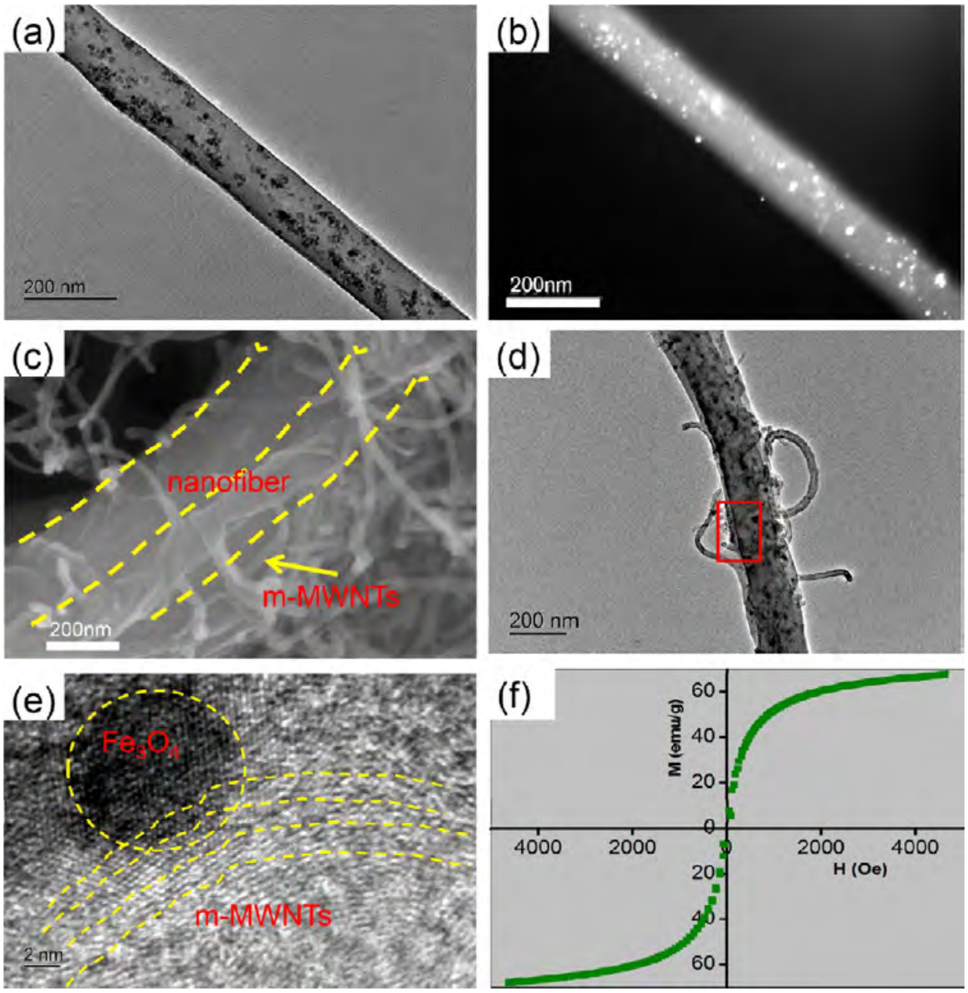

Figure 2. TEM, DFTEM, SEM, and HRTEM images of Fe_3O_4/PCL fibers and m-MWNT coated Fe_3O_4/PCL fibers. TEM (a) and DF TEM (b) images of Fe_3O_4/PCL fibers. SEM (c) and TEM (d) images of m-MWNT coated Fe_3O_4/PCL fibers. The yellow line indicates the Fe_3O_4/PCL fiber. (e) HRTEM image of the lattice of the Fe_3O_4 magnetic nanoparticles and m-MWNTs in the fiber matrix. The yellow line indicates the lattice of Fe_3O_4 and the m-MWNTs. (f) Magnetization hysteresis curve of the Fe_3O_4 magnetic nanoparticles.

the scrolled fiber mats is presented in Figure 1d. Additionally, Figure 1e shows a schematic of the fabrication of electrospinning ordered Fe_3O_4/PCL fiber composites coated with m-MWNTs. The vacuum-assisted spray technique was employed to obtain the m-MWNT coated Fe_3O_4/PCL fiber mats after electrospinning, effectively ensuring the alignment of the fibers and the good organization of the nanoparticles on each fiber, which impart better electrical conductivity and more stable magnetic force. Briefly, an electrospinning apparatus with a high speed roller was used to fabricate the flexible aligned Fe_3O_4/PCL fiber mats composed of organic polymer solution and magnetic nanoparticles dispersed in the solution. PCL was chosen as the polymer substrate due to its high chemical resistance, good tensile strength, great biocompatibility, and good mechanical stability. To spray the m-MWNTs onto the magnetic mats, the m-MWNTs were first dispersed in the absolute ethanol, and a certain proportion of methylene chloride was added to the m-MWNT suspensions. Ethanol was chosen as the solvent in which the m-MWNTs were dispersed because it could rapidly volatilize from the m-MWNT droplets by evaporating, leaving only the dispersed m-MWNTs on the Fe_3O_4/PCL nanofiber matrix. Methylene chloride was used to coagulate the m-MWNTs on the surface of the nanofibers and prevent the m-MWNTs from aggregating.

Furthermore, TEM, DFTEM, SEM, and HRTEM were combined to study the possible current producing mechanism of the m-MWNT coated Fe_3O_4/PCL fiber mats (Figure 2a–e). It is can be observed from Figure 2c,d that the m-MWNTs anchored onto the Fe_3O_4/PCL fiber. From the HRTEM image in Figure 2e, we can clearly find the crystal lattices of the magnetic nanoparticles and m-MWNTs crossed with each other, which will supply a channel for the electronic transport and thus contribute to the conductivity of the composites. Thus, the output current will be enhanced by several approaches. First, a coercive electric field will be produced by the external magnetic field due to the dipole interactions of the Fe_3O_4 magnetic nanoparticles.[46,47] Second, the magnetic flux density will be strengthened due to the perfect superparamagnetism of the Fe_3O_4 magnetic nanoparticles (Figure 2f). Finally, dipoles will be generated when the magnetic nanoparticles are aligned by an external magnetostatic field.[48]

To realize noninvasive electrical stimulation using an external power supply, an electric generating system was designed that mainly consisted of two parts: a rotating magnetic field and the conductive nanocomposites. The theory was important in that some physical variables cause a change in the electrical current produced by an external rotating magnetic field. In this paper, the output current produced by the rotating magnetic field

DOI: 10.1021/acsami.7b12854
ACS Appl. Mater. Interfaces 2017, 9, 38323−38335

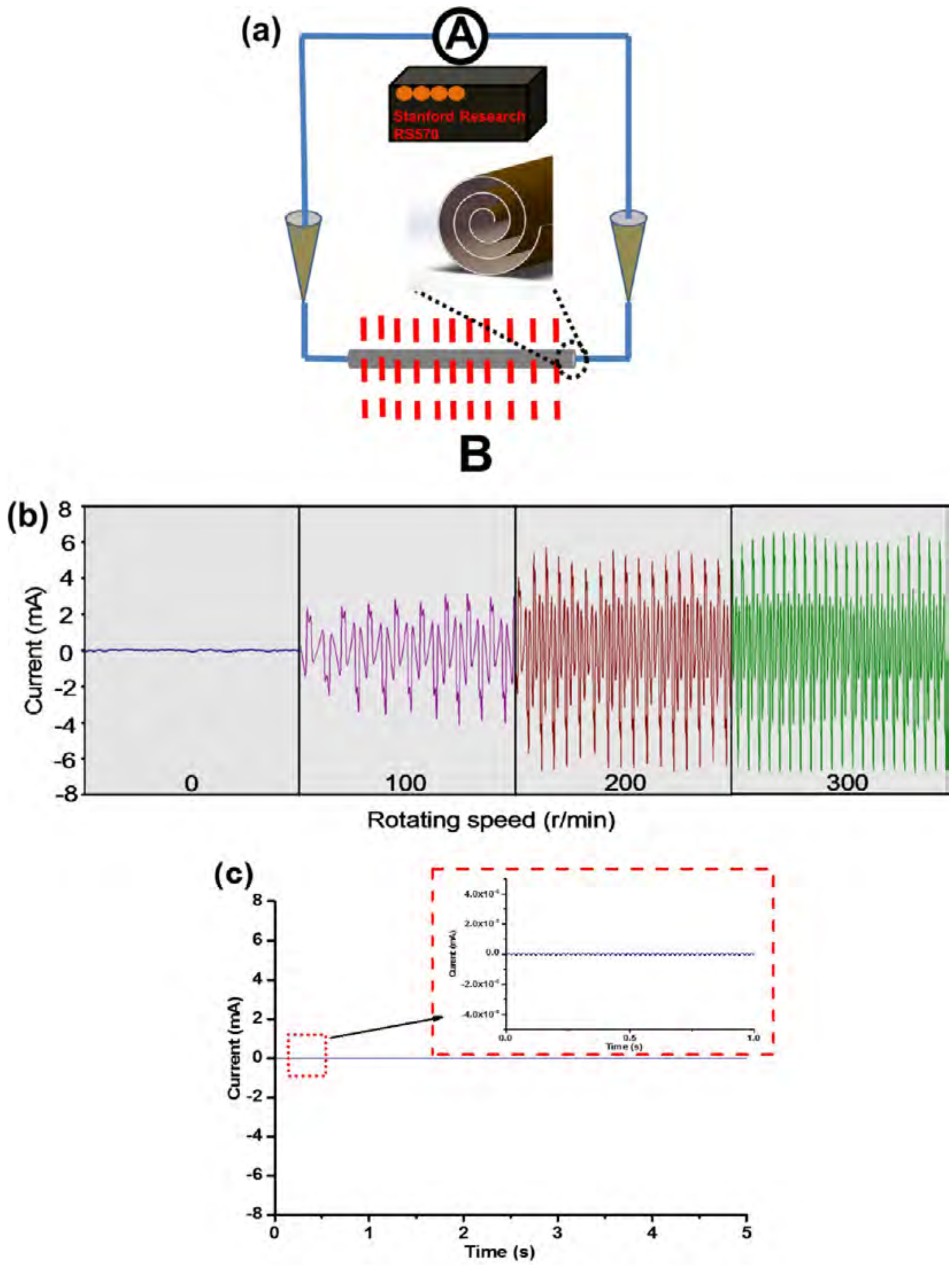

Figure 3. Design of the electromagnetic induction effect under external magnetic field. (a) Schematic illustration of an electric generating system that consists of an external rotating magnetic field, self-powered nanocomposites, and a measuring system. A Stanford Research RS570 is used as an ammeter in the measuring system. The cross section of the nanocomposites is also shown. (b) Short-circuit current (measured within 5 s) of a conductive copper stick under external magnetic induction lines with different rotation speeds (magnetic-cutting velocity) from 0 to 300 rpm. (c) Short-circuit current of insulative PCL sticks under the external magnetic induction lines with different rotation speeds.

depends on the changes in the magnetic flux (the rotating magnetic field strength is 300 mT). To prove the applicability of the self-designed electric generating system, conductive copper and insulative PCL sticks were employed simultaneously under the rotating magnetic field. The novel designed electric generating system, composed of an external rotating magnetic field, self-powered CNFs and a system for measuring current values, is shown in Figure 3a. A Stanford Research Systems RS570 was used as an ammeter. The cutting of the magnetic flux using the conductive copper sticks at different rotation speeds was measured by a low-noise current preamplifier. Short-circuit output currents were measured within 5 s and the rotation speed ranged from 0 to 300 rpm (Figure 3b). It is worth noting that a higher rotating speed can result in a higher electric output, reaching up to 2.2 mA when the rotation speed was 100 rpm. In addition, when the rotation

DOI: 10.1021/acsami.7b12854
ACS Appl. Mater. Interfaces 2017, 9, 38323−38335

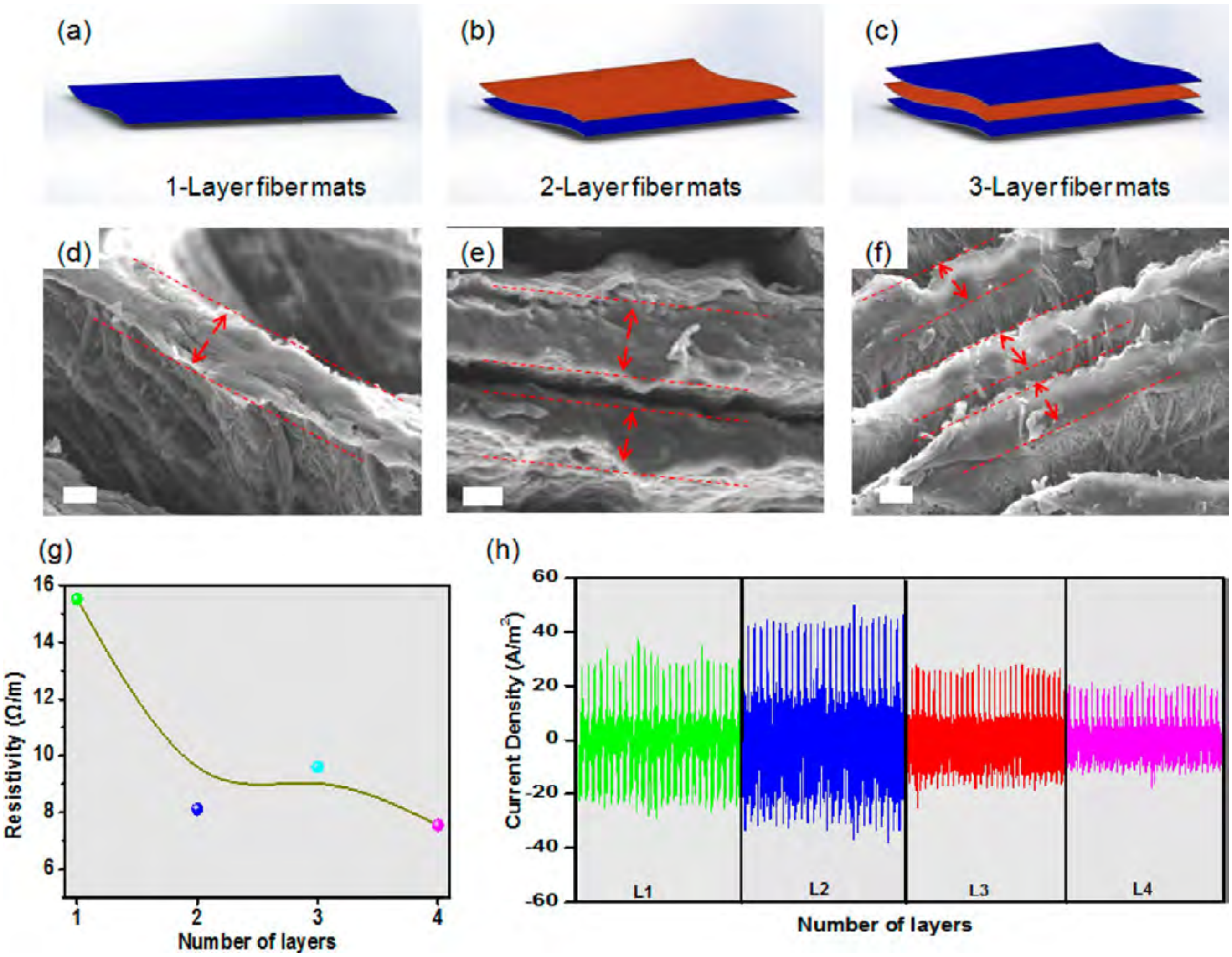

Figure 4. Performance characterization of the scrolled fiber mats with different layers. (a−c) Schematic models of m-MWNT coated Fe_3O_4/PCL fiber mats with one layer (a), two layers (b) and three layers (c). (d−f) Cross-sectional SEM images of the surface of the scrolled fiber mats with 1 layer (d) at a radius of 100 μm, 2 layers (e) at a radius of 200 μm, and 3 layers (f) at a radius of 300 μm, respectively. (g) Curve of resistivity of scrolled sticks prepared using m-MWNT coated Fe_3O_4/PCL fiber mats with different numbers of layers of. (h) Short-circuit current of mats with 1−4 layers. The scale bar is 10 μm.

speed was increased to 300 rpm, the short-circuit current reached up to 6.8 mA. However, absolutely no current was measured when the cutting stick was made of insulating PCL instead of conductive copper, as shown in Figure 3c. This result strongly proved that the self-designed electric generating system was feasible.

3.2. Influence of the Output Current of the Self-Powered Nanocomposites under an External Rotating Magnetic Field. Figure 4 presents the layers of m-MWNT coated Fe_3O_4/PCL fiber mats, as observed by cross-sectional SEM of the fracture surface of the scrolled fiber mats. Interestingly, the structure of the scrolled composite prepared by the curling of the m-MWNT coated Fe_3O_4/PCL fiber mats allows the fast transport of electrons.[49] As shown in Figure 4d−f, the radii of the scrolled mats are 100 μm for a 1-layer mat, 200 μm for a 2-layer mat, and 300 μm for a 3-layer mat, with an average layer thickness of is 18 ± 3 μm. Figure 4g shows the resistivity of scrolled sticks prepared using m-MWNTs coated Fe_3O_4/PCL fiber mats with different numbers of layers, demonstrating that the resistivity decreased from 15.52 Ω·m ($\rho = RS/L$, see detail calculation described above) for a 1-layer mat to 7.56 Ω·m for 4-layer mat. The decreased resistivity of the scrolled stick was due to the lowered number of discontinuous gaps and faster electron transport resulting from increasing the number of film layers. However, the current density of the scrolled stick was changed in a distinctive way (Figure 4h). It is obvious that the current density first increased and then decreased as the number of layers of the scrolled stick increased. In particular, at a rotating speed of 350 rpm the short-circuit current density of the 2-layer scrolled stick reached 42.8 A/m^2 ($C_d = I/S$, see detailed calculation procedure described above), while the current value of the 4-layer stick was 19.9 A/m^2. This phenomenon was consistent with the result discussed above and was due to the relationship with the intrinsic properties of the material. Hence, the effect on electronic transmission between layers and the current density decreased as the cross section of the material became larger.

Scrolled fiber mats with multiple layers were also used. Regarding these multilayer m-MWNTs coated Fe_3O_4/PCL fiber mats, the characteristics between layers were examined and are shown in Figure S4. FE-SEM images (Figure S4a,b) show that the m-MWNTs were anchored and well dispersed on

DOI: 10.1021/acsami.7b12854
ACS Appl. Mater. Interfaces 2017, 9, 38323−38335

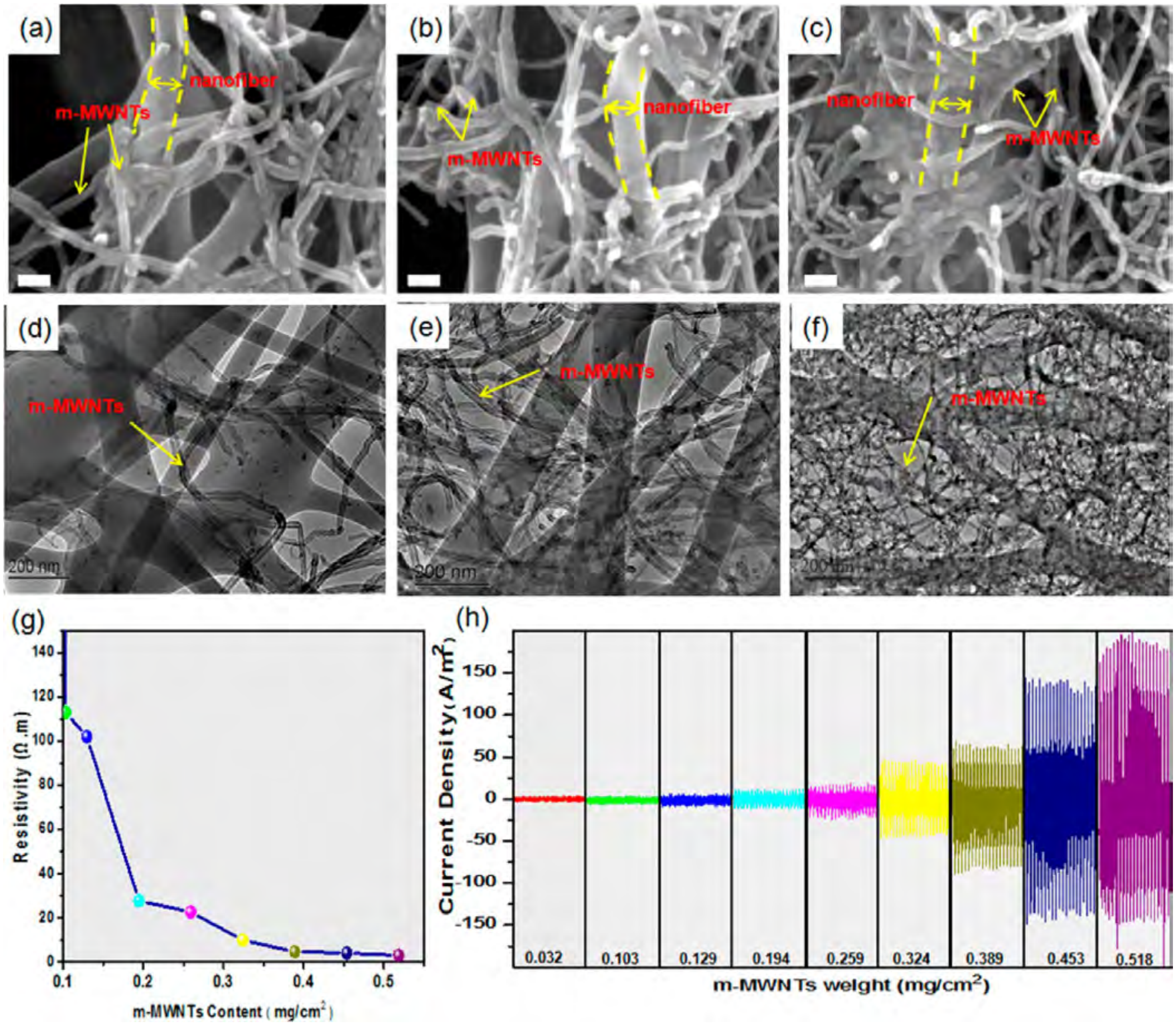

Figure 5. (a–c) FE-SEM and (d–f) FE-TEM images of Fe_3O_4/PCL nanofiber composites coated with different cumulative weight of m-MWNTs. (a, d) 0.032 mg/cm^2, (b, e) 0.129 mg/cm^2, and (c, f) 0.259 mg/cm^2. The scale-bar is 200 nm. (g) Curve of resistivity [Ω·m] of scrolled stick prepared using Fe_3O_4/PCL fiber mats coated with different cumulative weight of m-MWNTs. (h) Short-circuit current of Fe_3O_4/PCL fibers coated with different cumulative weight of m-MWNTs.

the Fe_3O_4/PCL fiber mats. The characteristics between layers are shown in Figure S4c–f. It can be concluded that the carbon nanotubes were connected between two layers. We presumed that the m-MWNTs play a key role in enhancing the electron transfer ability and reinforcing the conductivity of the CNFs. The m-MWNTs were connected between two layers because of the hydrophilicity/hydrophobicity of the species, the absorption of the m-MWNT surfaces, the carboxyl groups on Fe_3O_4 and those on the m-MWNTs forming hydrogen bonds, and the adhesion of the m-MWNTs after acid treatment.

The use of the electromagnetic induction effect to generate an electric signal was closely related to the structure of the m-MWNTs combined with the magnetic fiber mats. The output performance of different cumulative weights of m-MWNTs coated onto the Fe_3O_4/PCL fibers is shown in Figure 5. Because of the lowered density of the network of the m-MWNTs on the matrix, the conductivity of the scrolled stick also decreased. In contrast, with more m-MWNTs, the discontinuous spaces between fibers will decrease due to the existence of the network structure of the m-MWNTs anchored on and intertwined around the Fe_3O_4/PCL fibers (Figure 5b,c and S5b,c). As FE-TEM images shown in Figure 5d–f, the different cumulative weight of m-MWNTs also demonstrated the uniform distribution in Fe_3O_4/PCL nanofiber composites. The resistivity of the scrolled sticks obviously decreases with the increasing content of the m-MWNTs, as shown in Figure 5g. Resistivity decreased dramatically when the content of m-MWNTs reached 0.194 mg/cm^2, indicating that the m-MWNTs enhanced the conductivity of the scrolled stick. Meanwhile, the electric output of m-MWNT coated Fe_3O_4/PCL fiber mats was highly related to the content of m-MWNTs such that the current amplitude rose gradually with the increase in m-MWNT content, as shown in Figure 5h. For example, there was almost no current when the Fe_3O_4/PCL fiber mats

DOI: 10.1021/acsami.7b12854
ACS Appl. Mater. Interfaces 2017, 9, 38323–38335

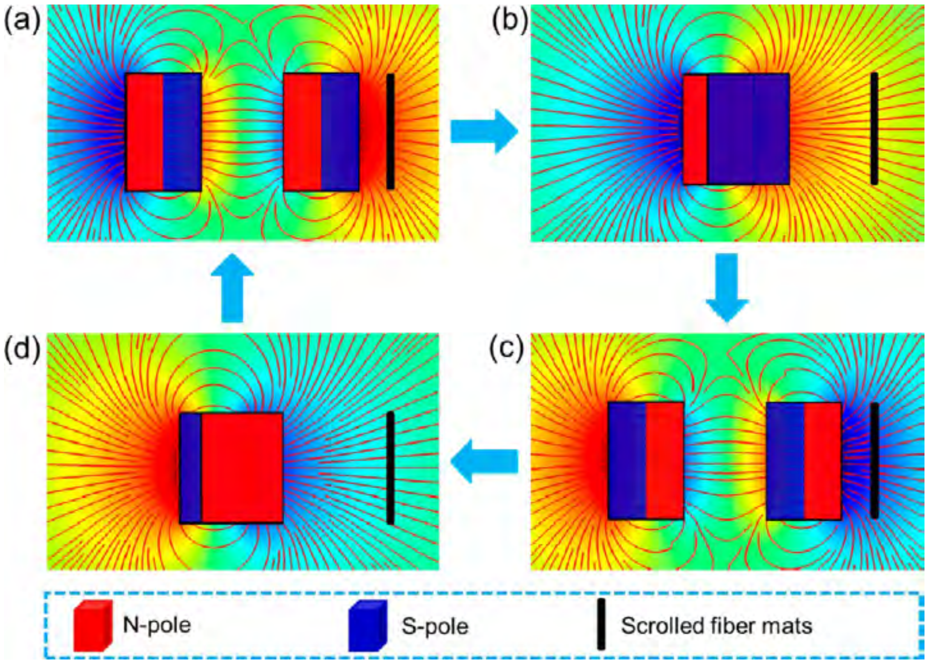

Figure 6. Working principle of the self-powered scrolled fiber mats under an external rotating magnetic field; COMSOL simulation was employed for visualization. (a) Magnetic field in the nature stage, (b) $^1/_4$ cycle, (c) $^1/_2$ cycle, and (d) $^3/_4$ cycle.

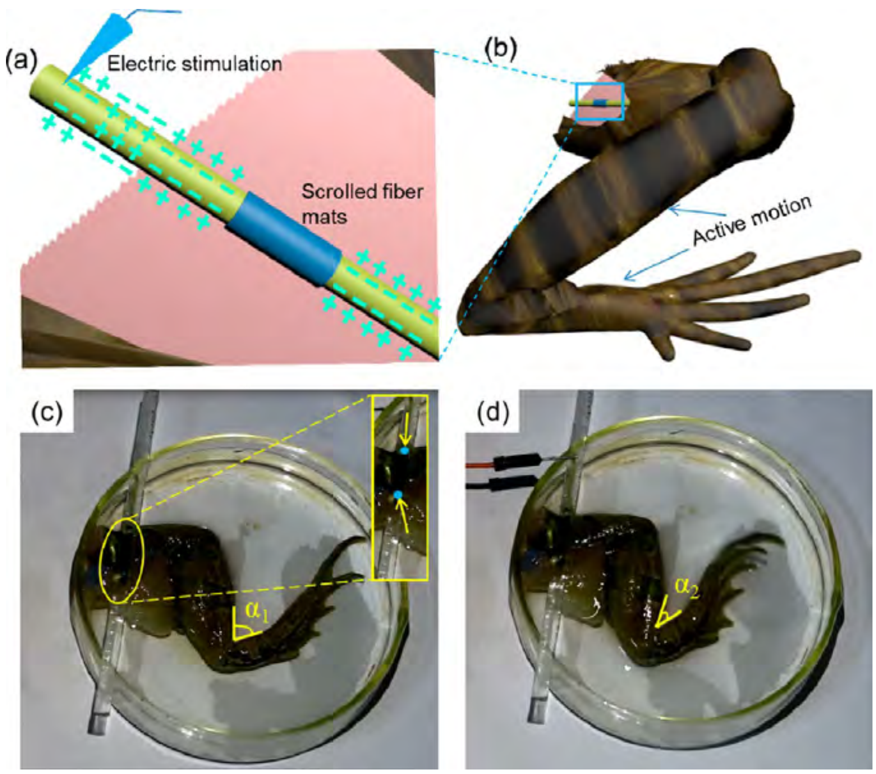

Figure 7. Demonstration of m-MWNT coated Fe_3O_4/PCL fiber mats replacing the injured nerve and realization of nerve stimulation. (a) Schematic diagram of the nanofiber composites replacing the injured nerve and the local current flowing inside the nerve. (b) Schematic diagram of a bullfrog's hind limb with the sciatic nerve exposed and the injured part replaced by m-MWNT coated Fe_3O_4/PCL nanofiber composites. (c, d) Picture of a bullfrog's hind limb with the sciatic nerve exposed and the injured part replaced by m-MWNT coated Fe_3O_4/PCL nanofiber composites before electric stimulation (c) and after electric stimulation (d). We used an alpha angle (α) to characterize the instantaneous change in muscle shape as a result of the electric stimulation: $\alpha_1 > \alpha_2$.

were coated with 0.032 and 0.103 mg/cm^2 MWNTs, while the current density was 3.18 A/m^2 when the mats were coated with 0.129 mg/cm^2 m-MWNTs. Moreover, the CNFs could reach up to 191.1 A/m^2 when the content of m-MWNTs was 0.518 mg/cm^2, showing an obvious increase in the output current density. Thus, the amount of m-MWNTs was the important

DOI: 10.1021/acsami.7b12854
ACS Appl. Mater. Interfaces 2017, 9, 38323−38335

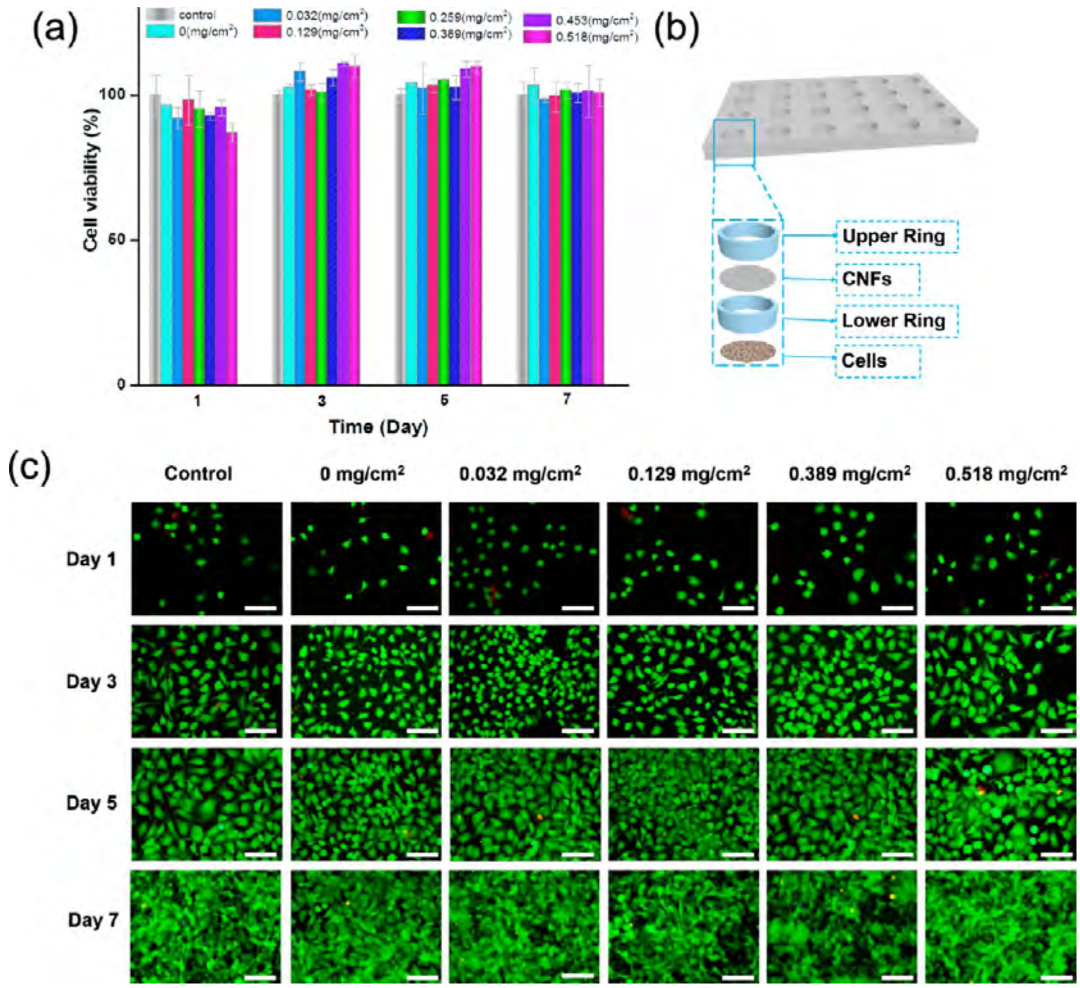

Figure 8. (a) Viability of EC cells cultured with Fe_3O_4/PCL nanofibers coated with different cumulative weights [mg/cm^2] of m-MWNTs for 7days. (b) Schematic illustration of the cell culture. After the cells were attached and spread well, the fiber meshes were added and fixed in the middle of the ring. (c) Live/dead staining of captured EC cells on different samples (containing Fe_3O_4/PCL nanofibers coated with different cumulative weight [mg/cm^2] of m-MWNTs) after further incubation for 1, 3, 5, and 7 days. Scale bar = 80 μm.

factor contributing to the conductivity of the self-powered composite.

As mentioned above, m-MWNTs adhere and anchor on to fibers, which is shown in Figures 5a−f and S5a−c. This distinct interfacial interaction behavior can be attributed to the surfaces of the m-MWNTs and polymer nanofibers. The pristine m-MWNTs were easily phase-separated and agglomerated out of the polymer matrix. On the one hand, the PCL fibers and m-MWTNs possessed a smaller contact angle due to the mixed solution spray; on the other hand, the hydrophilicity/hydrophobicity of the species, the absorption of the m-MWNT surfaces, the carboxyl groups on Fe_3O_4 and carboxyl groups on the m-MWNTs forming hydrogen bonds, and the adhesion of the m-MWNTs after acid treatment enabled their good dispersion in the matrix. In this case, the m-MWNTs were more likely to be embedded into the Fe_3O_4/PCL nanofiber.

3.3. Working Principle of Self-Powered Nanocomposites under an External Rotating Magnetic Field. Figure 6 illustrates the simulated electricity generation based on the working principle of the CNFs under an external rotating magnetic field via Multiphysics COMSOL software. First, from the nature stage to the $^1/_4$ cycle, the magnetic flux density would decrease when the magnetic field rotated, resulting in a lower current value. Furthermore, the magnetic field rotating from the $^1/_4$ to the $^1/_2$ cycle led to a continuous increase in the magnetic flux density. At the same time, with the magnetic field rotating to the $^1/_2$ cycle, an increase of the magnetic flux density with opposite polarization would induce a negative current in the nanocomposites. The magnetic flux density would also keep decreasing as the magnetic field rotated from the $^1/_2$ cycle to the $^3/_4$ cycle. Finally, from the $^3/_4$ cycle to the nature stage, a decrease in the flux density induced a lower current value. This is a full cycle of the electricity-generating process (Video S1).

3.4. CNFs Replace an Injured Nerve to Realize Functional Electrical Stimulation. To demonstrate the nerve stimulation ability of the m-MWNT coated Fe_3O_4/PCL fiber mats replacing an injured nerve, functional electrical stimulation (FES) of a bullfrog's sciatic nerve was carried out. We successfully achieved real-time FES using using the composites in place of an injured nerve. It could be proved that the nanocomposite was suitable for replacing an injured nerve as shown in Figure 7, which shows a schematic diagram of the enlarged view of the two injured nerve connected by scrolled fiber mats (Figure 7b) and the local current flowing inside the nerve (Figure 7a). Throughout the experiment, the nerve was kept wet by Ringer's solution for amphibians.[13] Under the instantaneous electrical input, vibrant foot twitching

DOI: 10.1021/acsami.7b12854
ACS Appl. Mater. Interfaces 2017, 9, 38323−38335

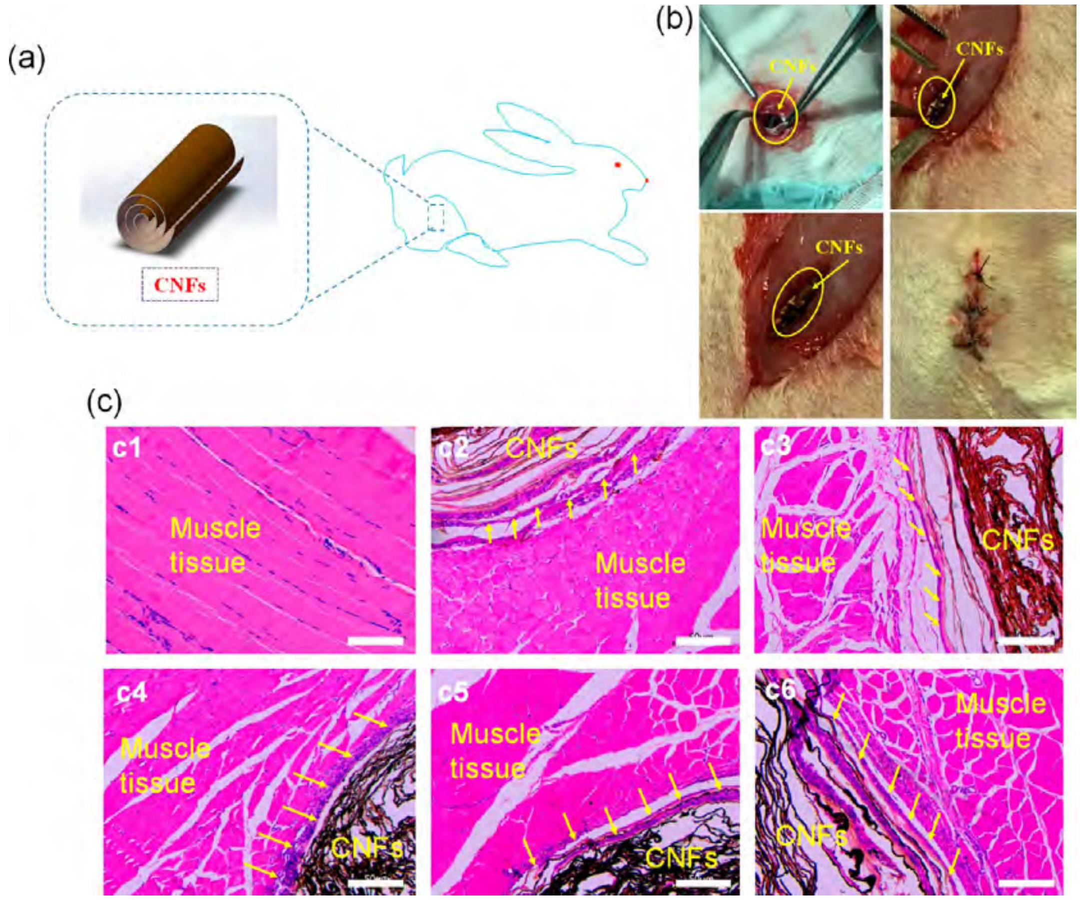

Figure 9. *In vivo* muscular implant test on a rabbit's hind limb with different samples (CNFs containing different cumulative weights [mg/cm^2] of m-MWNTs) after 4 weeks. (a) Schematic illustration of the muscular implant test on a rabbit's hind limb. (b) Surgical procedure of the muscular implantation. (c) Representative micrographs of hematoxylin/eosin (HE) stained sections at 4 weeks after implantation. (c1) Control group, (c2) 0.032 mg/cm^2, (c3) 0.259 mg/cm^2, (c4) 0.389 mg/cm^2, (c5) 0.453 mg/cm^2, and (c6) 0.518 mg/cm^2 (magnification ×50). The yellow arrow indicates for granulation tissue. White scale bar = 50 μm.

was observed, resulting from the contraction of the gastrocnemius muscle, as visualized in Figure 7c,d. The foot twitching was perfectly synchronized (Video S2), indicating the real-time stimulation of the m-MWNT coated Fe_3O_4/PCL fiber mats replacing the injured nerve. In fact, we have used the CNFs and insulative PCL stick to replace the injured nerve, respectively. The latter is the control group. As a result, no instantaneous change in muscle shape as a result of the electric stimulation was observed when the material replacing the injured nerve was made of insulating PCL instead of CNFs. It should be noted that since the action potential of the bullfrog's sciatic nerve ranged from −60 to −80 mV, a voltage input of at least 50 mV at 1 Hz was necessary for innervation of the sciatic nerve.[50,51] The current value means that it was limit for the m-MWNT coated Fe_3O_4/PCL fiber mats to power the FES of a sciatic nerve of a bullfrog. A power source was applied to achieve FES using the nanocomposites.

3.5. Cytotoxicity Assay. The cytotoxicity of the CNFs with different cumulative weights of m-MWNTs was assessed by an Alamar Blue assay, Figure 8a shows the viability of ECs incubated with different samples. As shown in the picture, it is obvious that the cell viability for all samples was more than 90% after 1, 3, 5, and 7 days of culture. After 7 days of cell culture, the samples also show excellent biocompatibility, indicating that both Fe_3O_4 and the m-MWNTs in the CNFs composites exhibited desirable biocompatibility. Meanwhile, the cytotoxicity of the CNFs was evaluated by optical microscopy analysis. Representative fluorescence images are shown in Figures 8c and S9. From these pictures, it is evident that the cells in CNF group grew as well as those in the control group. Even after incubation for 7 days, all cells grown in the CNF group were similar to the control group. These results were in agreement with an Alamar Blue assay, which strongly proved that the CNFs with different cumulative weights of m-MWNTs always have excellent biocompatibility and suggests that the m-MWNTs and the Fe_3O_4 in the CNFs composites were almost nontoxic.[37,38]

3.6. *In Vivo* Implantation. *In vivo* muscle implantation experiments were further used to evaluate the biocompatibility and tissue integration ability of the CNFs, as shown in Figure 9. A muscular implant test was carried out on a rabbit's hind limb with different samples. Figure 9a shows a schematic of the muscular implantation, and Figure 9b shows the surgical procedure of the muscular implantation.

Histological analysis was further used to assess the interface between the CNFs and musculature. Compared with the control group, the CNF groups displayed newly formed granulation tissue. Granulation tissue formation from the wound edge in the musculature is a common phenomenon during an implantation procedure. A wound healing response continuum at the implantation site was triggered by the injury during the surgical procedure.[52,53] Granulation tissue is a stage

DOI: 10.1021/acsami.7b12854
ACS Appl. Mater. Interfaces 2017, 9, 38323−38335

of the wound healing cascade that indicates inflammation resolution, which is further evidenced by the presence of fibroblast infiltration in the CNF groups. Additionally, for the CNFs coated with fewer m-MWNTs, no foreign body giant cells or necrotic muscle tissues were observed (Figure 9c2−c5). For the CNFs coated with more m-MWNTs (0.518 mg/cm^2), fibroblasts and a few foreign body giant cells were observed in the granulation tissue (Figure 9c6). All the CNFs groups showed fibroblast cells with good morphology and no necrotic muscle tissues. A hallmark of the final stages of wound healing cascade is a mature fibrous capsule.[52] Thin fibrous capsules could be seen after 4 weeks in the CNF groups. Overall, the CNFs coated with fewer m-MWNTs showed great biocompatibility and well-grown fibroblast cells without necrotic muscle tissue, muscle or even a foreign body reaction after 4 weeks.

On the basis of the electromagnetic induction effect, the designed self-powered nanocomposites could generate power when an external magnetic field was applied to the CNFs. The requirement of an external power source in the electrical stimulation process is inconvenient in biomedical application. This work paves the way to boost the electrical stimulation in a more convenient manner. In a proper power consumption environment, the composites prepared in this paper can be used. The results prove that the method of preparing the conductive m-MWNT coated Fe_3O_4/PCL composites and the electric generating system of the current values are entirely feasible and valuable in many potential fields, such as neurotransmission. Moreover, it is important that the current is generated under an external magnetic field instead of using external power voltage.

4. CONCLUSION

We have designed and fabricated self-powered CNFs consisting of m-MWNTs, superparamagnetic Fe_3O_4 nanoparticles and PCL nanofibers. The magnetic nanoparticles loaded into the electrospinning nanofibers can both strengthen the magnetic flux density effectively and enhance the conductive properties of the nanocomposites as an external magnetic field is applied. The output current density from cutting the magnetic flux can reach up to 191.1 A/m^2 under an external magnetic field. Furthermore, the method of generating current from the CNF using an external magnetic field in low-power consumption and unique environments can achieve when the CNFs replaced a bullfrog's sciatic nerve. The CNFs possessed excellent cytotoxicity and good enough biocompatibility to be implanted *in vivo* without causing any inflammation. We believe that the nanocomposite and the power generation method may be applicable as a noninvasive power supply for electric stimulation, although considerable work will be necessary to further utilize the nanocomposite in special work environments in the future.

■ ASSOCIATED CONTENT

Supporting Information

The Supporting Information is available free of charge on the ACS Publications website at DOI: 10.1021/acsami.7b12854.

Additional information includes materials and device fabrication, TEM images, EDS mapping and SEM images of Fe_3O_4/PCL fibers, XRD patterns and FT-IR of m-MWNTs coated Fe_3O_4/PCL nanofiber mats, m-MWNTs and Fe_3O_4. Schematic illustration of the conductivity mechanism of the electromagnetic induction effect under external magnetic field.(PDF)

Video S1: electrical output performance of the scrolled sticks. A full cycle of the electricity-generating process (AVI)

Video S2: functional electrical stimulation of the nanocomposites replacing the bullfrog's injured nerve (AVI)

■ AUTHOR INFORMATION

Corresponding Authors

*Tel.: 86-28-87600896. E-mail: zxtwin@sina.com.

*Tel.: 86-28-87600415. E-mail: wqyang@swjtu.edu.cn.

ORCID

Xiaotong Zheng: 0000-0003-0489-3339

Weiqing Yang: 0000-0001-8828-9862

Notes

The authors declare no competing financial interest.

■ ACKNOWLEDGMENTS

This work was supported by National Natural Science Foundation of China under Grant (51203130), the Central Universities under Grant (2682013CX001), and Sichuan Province Youth Science and Technology Innovation Team (Grant No. 2016TD0026).

■ REFERENCES

(1) Hsiao, Y. S.; Liao, Y. H.; Chen, H. L.; Chen, P. L.; Chen, F. C. Organic Photovoltaics and Bioelectrodes Providing Electrical Stimulation for PC12 Cell Differentiation and Neurite Outgrowth. *ACS Appl. Mater. Interfaces* **2016**, *8*, 9275−9284.

(2) Zhu, B.; Luo, S. C.; Zhao, H. C.; Lin, H. A.; Sekine, J.; Nakao, A.; Chen, C.; Yamashita, Y.; Yu, H. H. Large Enhancement in Neurite Outgrowth on a Cell Membrane-Mimicking Conducting Polymer. *Nat. Commun.* **2014**, *5*, 4523.

(3) Kim, I.; Lee, H. Y.; Kim, H.; Lee, E.; Jeong, D. W.; Kim, J. J.; Park, S. H.; Ha, Y.; Na, J.; Chae, Y.; et al. Enhanced Neurite Outgrowth by Intracellular Stimulation. *Nano Lett.* **2015**, *15*, 5414−5419.

(4) Quigley, A. F.; Razal, J. M.; Kita, M.; Jalili, R.; Gelmi, A.; Penington, A.; Ovalle-Robles, R.; Baughman, R. H.; Clark, G. M.; Wallace, G. G.; et al. Electrical Stimulation of Myoblast Proliferation and Differentiation on Aligned Nanostructured Conductive Polymer Platforms. *Adv. Healthcare Mater.* **2012**, *1*, 801−808.

(5) Márquez-Ruiz, J.; Ammann, C.; Leal-Campanario, R.; Ruffini, G.; Gruart, A.; Delgado-Garcia, J. M. Synthetic Tactile Perception Induced by Transcranial Alternating-Current Stimulation can Substitute for Natural Sensory Stimulus in Behaving Rabbits. *Sci. Rep.* **2016**, *6*, 19753.

(6) Ud-Din, S.; Sebastian, A.; Giddings, P.; Colthurst, J.; Whiteside, S.; Morris, J.; Nuccitelli, R.; Pullar, C.; Baguneid, M.; Bayat, A. Angiogenesis is Induced and Wound Size is Reduced by Electrical Stimulation in an Acute Wound Healing Model in Human Skin. *PLoS One* **2015**, *10*, e0124502.

(7) Leppik, L. P.; Froemel, D.; Slavici, A.; Ovadia, Z. N.; Hudak, L.; Henrich, D.; Marzi, I.; Barker, J. H. Effects of Electrical Stimulation on Rat Limb Regeneration, a New Look at an Old Model. *Sci. Rep.* **2016**, *5*, 18353.

(8) Eng, G.; Lee, B.; Protas, L.; Gagliardi, M.; Brown, K.; Kass, R. S.; Keller, G.; Robinson, R. B.; Vunjak-Novakovic, G. Autonomous Beating Rate Adaptation in Human Stem Cell-Derived Cardiomyocytes. *Nat. Commun.* **2016**, *7*, 10312.

(9) Huang, Y. J.; Wu, H. C.; Tai, N. H.; Wang, T. W. Carbon Nanotube Rope with Electrical Stimulation Promotes the Differ-

entiation and Maturity of Neural Stem Cells. *Small* **2012**, *8*, 2869−2877.

(10) Vitale, F.; Summerson, S. R.; Aazhang, B.; Kemere, C.; Pasquali, M. Neural Stimulation and Recording with Bidirectional, Soft Carbon Nanotube Fiber Microelectrodes. *ACS Nano* **2015**, *9*, 4465−4474.

(11) Min, Y.; Yang, Y. Y.; Poojari, Y.; Liu, Y. D.; Wu, J. C.; Hansford, D. J.; Epstein, A. J. Sulfonated Polyaniline-Based Organic Electrodes for Controlled Electrical Stimulation of Human Osteosarcoma Cells. *Biomacromolecules* **2013**, *14*, 1727−1731.

(12) Zhu, G.; Wang, A. C.; Liu, Y.; Zhou, Y. H.; Wang, Z. L. Functional Electrical Stimulation by Nanogenerator with 58 V Output Voltage. *Nano Lett.* **2012**, *12*, 3086−3090.

(13) Laocharoensuk, R.; Burdick, J.; Wang, J. Carbon-Nanotube-Induced Acceleration of Catalytic Nanomotors. *ACS Nano* **2008**, *2*, 1069−1075.

(14) Vilela, D.; Parmar, J.; Zeng, Y. F.; Zhao, Y. L.; Sanchez, S. Graphene-Based Microbots for Toxic Heavy Metal Removal and Recovery from Water. *Nano Lett.* **2016**, *16*, 2860−2866.

(15) Thrivikraman, G.; Lee, P. S.; Hess, R.; Haenchen, V.; Basu, B.; Scharnweber, D. Interplay of Substrate Conductivity, Cellular Microenvironment, and Pulsatile Electrical Stimulation toward Osteogenesis of Human Mesenchymal Stem Cells in Vitro. *ACS Appl. Mater. Interfaces* **2015**, *7*, 23015−23028.

(16) Ho, D.; Zou, J. L.; Chen, X. J.; Munshi, A.; Smith, N. M.; Agarwal, V.; Hodgetts, S. I.; Plant, G. W.; Bakker, A. J.; Harvey, A. R.; et al. Hierarchical Patterning of Multifunctional Conducting Polymer Nanoparticles as a Bionic Platform for Topographic Contact Guidance. *ACS Nano* **2015**, *9*, 1767−1774.

(17) Yan, L.; Zhao, B. X.; Liu, X. H.; Li, X.; Zeng, C.; Shi, H. Y.; Xu, X. X.; Lin, T.; Dai, L. M.; Liu, Y. Aligned Nanofibers from Polypyrrole/Graphene as Electrodes for Regeneration of Optic Nerve via Electrical Stimulation. *ACS Appl. Mater. Interfaces* **2016**, *8*, 6834−6840.

(18) Chen, J.; Huang, Y.; Zhang, N. N.; Zou, H. Y.; Liu, R. Y.; Tao, C. Y.; Fan, X.; Wang, Z. L. Micro-cable Structured Textile for Simultaneously Harvesting Solar and Mechanical Energy. *Nat. Energy* **2016**, *1*, 16138.

(19) Zhang, N. N.; Chen, J.; Huang, Y.; Guo, W. W.; Yang, J.; Du, J.; Fan, X.; Tao, C. Y. A Wearable All-Solid Photovoltaic Textile. *Adv. Mater.* **2016**, *28*, 263−269.

(20) Yang, W. Q.; Chen, J.; Wen, X. N.; Jing, Q. S.; Yang, J.; Su, Y. J.; Zhu, G.; Wu, W. Z.; Wang, Z. L. Triboelectrification Based Motion Sensor for Human-Machine Interfacing. *ACS Appl. Mater. Interfaces* **2014**, *6*, 7479−7484.

(21) Zhang, L.; Jin, L.; Zhang, B. B.; Deng, W. L.; Pan, H.; Tang, J. F.; Zhu, M. H.; Yang, W. Q. Multifunctional Triboelectric Nanogenerator Based on Porous Micro-Nickel Foam to Harvest Mechanical Energy. *Nano Energy* **2015**, *16*, 516−523.

(22) Yang, J.; Chen, J.; Su, Y. J.; Jing, Q. S.; Li, Z. L.; Yi, F.; Wen, X. N.; Wang, Z. N.; Wang, Z. L. Eardrum-Inspired Active Sensors for Self-Powered Cardiovascular System Characterization and Throat-Attached Anti-Interference Voice Recognition. *Adv. Mater.* **2015**, *27*, 1316−1326.

(23) Bai, P.; Zhu, G.; Jing, Q. S.; Yang, J.; Chen, J.; Su, Y. J.; Ma, J. S.; Zhang, G.; Wang, Z. L. Membrane-Based Self-Powered Triboelectric Sensors for Pressure Change Detection and Its Uses in Security Surveillance and Healthcare Monitoring. *Adv. Funct. Mater.* **2014**, *24*, 5807−5813.

(24) Wang, Z. L.; Chen, J.; Lin, L. Progress in Triboelectric Nanogenertors as New Energy Technology and Self-Powered Sensors. *Energy Environ. Sci.* **2015**, *8*, 2250−2282.

(25) Lee, M.; Bae, J.; Lee, J.; Lee, C. S.; Hong, S.; Wang, Z. L. Self-Powered Environmental Sensor System Driven by Nanogenerators. *Energy Environ. Sci.* **2011**, *4*, 3359−3363.

(26) Wang, Z. L. Self-Powered Nanotech-Nanosize Machines Need Still Tinier Power Plants. *Sci. Am.* **2008**, *298*, 82−87.

(27) Wang, X.; Wang, S. H.; Yang, Y.; Wang, Z. L. Hybridized Electromagnetic-Triboelectric Nanogenerator for Scavenging Air-Flow Energy to Sustainably Power Temperature Sensors. *ACS Nano* **2015**, *9*, 4553−4562.

(28) Fan, F. R.; Tang, W.; Yao, Y.; Luo, J. J.; Zhang, C.; Wang, Z. L. Complementary Power Output Characteristics of Electromagnetic Generators and Triboelectric Generators. *Nanotechnology* **2014**, *25*, 135402.

(29) Quan, T.; Wang, X.; Wang, Z. L.; Yang, Y. Hybridized Electromagnetic−Triboelectric Nanogenerator for a Self-Powered Electronic Watch. *ACS Nano* **2015**, *9*, 12301−12310.

(30) Zhang, K. W.; Wang, X.; Yang, Y.; Wang, Z. L. Hybridized Electromagnetic-Triboelectric Nanogenerator for Scavenging Biomechanical Energy for Sustainably Powering Wearable Electronics. *ACS Nano* **2015**, *9*, 3521−3529.

(31) Cheng, R.; Huang, W. J.; Huang, L. J.; Yang, B.; Mao, L. D.; Jin, K. L.; ZhuGe, Q.; Zhao, Y. P. Acceleration of Tissue Plasminogen Activator-Mediated Thrombolysis by Magnetically Powered Nanomotors. *ACS Nano* **2014**, *8*, 7746−7754.

(32) Gao, W.; Sattayasamitsathit, S.; Manesh, K. M.; Weihs, D.; Wang, J. Magnetically Powered Flexible Metal Nanowire Motors. *J. Am. Chem. Soc.* **2010**, *132*, 14403−14405.

(33) Yamaguchi, M.; Ito, A.; Ono, A.; Kawabe, Y.; Kamihira, M. Heat-Inducible Gene Expression System by Applying Alternating Magnetic Field to Magnetic Nanoparticles. *ACS Synth. Biol.* **2014**, *3*, 273−279.

(34) Zhang, C.; Tang, W.; Han, C. B.; Fan, F. R.; Wang, Z. L. Theoretical Comparison, Equivalent Transformation, and Conjunction Operations of Electromagnetic Induction Generator and Triboelectric Nanogenerator for Harvesting Mechanical Energy. *Adv. Mater.* **2014**, *26*, 3580−3591.

(35) Zhou, S. B.; Deng, X. M.; Yang, H. Biodegradable Poly(ε-caprolactone)-poly(ethylene glycol) Block Copolymers: Characterization and Their Use as Drug Carriers for a Controlled Delivery system. *Biomaterials* **2003**, *24*, 3563−3570.

(36) Zheng, X. T.; Zhou, S.; Xiao, Y.; Yu, X.; Li, X.; Wu, P. Shape Memory Effect of Poly(D,L-lactide)/Fe_3O_4 Nanocomposites by Inductive Heating of Magnetite Particles. *Colloids Surf., B* **2009**, *71*, 67−72.

(37) Gong, T.; Li, W. B.; Chen, L. W.; Wang, L.; Shao, S. J.; Zhou, S. B. Remotely Actuated Shape Memory Effect of Electrospun Composite Nanofibers. *Acta Biomater.* **2012**, *8*, 1248−1259.

(38) Xiao, Y.; Gong, T.; Zhou, S. B. The Functionalization of Multi-walled Carbon Nanotubes by in Situ Deposition of Hydroxyapatite. *Biomaterials* **2010**, *31*, 5182−5190.

(39) Shao, S. J.; Zhou, S. B.; Li, L.; Li, J. R.; Luo, C.; Wang, J. X.; Li, X. H.; Weng, J. Osteoblast Function on Electrically Conductive Electrospun PLA/MWCNTs Nanofibers. *Biomaterials* **2011**, *32*, 2821−2833.

(40) Zhang, H.; Liu, Y.; Kuwata, M.; Bilotti, E.; Peijs, T. Improved Fracture Toughness and Integrated Damage Sensing Capability by Spray Coated CNTs on Carbon Fibre Prepreg. *Composites, Part A* **2015**, *70*, 102−110.

(41) Saetia, K.; Schnorr, J. M.; Mannarino, M. M.; Kim, S. Y.; Rutledge, G. C.; Swager, T. M.; Hammond, P. T. Spray-Layer-by-Layer Carbon Nanotube/Electrospun Fiber Electrodes for Flexible Chemiresistive Sensor Applications. *Adv. Funct. Mater.* **2014**, *24*, 492−502.

(42) Yang, G.; Wang, J.; Wang, Y.; Li, L.; Guo, X.; Zhou, S. B. An Implantable Active-Targeting Micelle-in-Nanofiber Device for Efficient and Safe Cancer Therapy. *ACS Nano* **2015**, *9*, 1161−1174.

(43) Gillette, R. H.; Sherman, A. The Nature of the Hydrogen Bond. I. Association in Carboxylic Acids. *J. Am. Chem. Soc.* **1936**, *58*, 1135−1139.

(44) Zhang, X.; Chen, T.; Yan, H. J.; Wang, D.; Fan, Q. H.; Wan, L. J.; Ghosh, K.; Yang, H. B.; Stang, P. J. Hydrogen Bond Partner Reorganization in the Coadsorption of a Monodendron and Pyridylethynyl Derivatives. *Langmuir* **2011**, *27*, 1292−1297.

(45) Xuyen, T. N.; Kim, H. T.; Geng, H. Z.; Lee, H. I.; Kim, K. K.; Lee, Y. H. Three-dimensional Architecture of Carbon Nanotube-anchored Polymer Nanofiber C. *J. Mater. Chem.* **2009**, *19*, 7822−7825.

(46) Mørup, S.; Hansen, M. F.; Frandsen, C. Magnetic Interactions Between Nanoparticles. *Beilstein J. Nanotechnol.* **2010**, *1*, 182−190.
(47) Hwang, J. G.; Zahn, M.; O'Sullivan, F. M.; Pettersson, L. A. A.; Hjortstam, O.; Liu, R. Liu R. S. Effects of Nanoparticle Charging on Streamer Development in Transformer Oil-Based Nanofluids. *J. Appl. Phys.* **2010**, *107*, 014310.
(48) Zhang, W. X.; Sun, J. F.; Bai, T. T.; Wang, C. Y.; Zhuang, K. K.; Zhang, Y.; Gu, N. Quasi-One-Dimensional Assembly of Magnetic Nanoparticles Induced by a 50 Hz Alternating Magnetic Field. *ChemPhysChem* **2010**, *11*, 1867−1870.
(49) Kwon, C. H.; Lee, S. H.; Choi, Y. B.; Lee, J. A.; Kim, S. H.; Kim, H. H.; Spinks, G. M.; Wallace, G. G.; Lima, M. D.; Kozlov, M. E.; et al. High-Power Biofuel Cell Textiles from Woven Biscrolled Carbon Nanotube Yarns. *Nat. Commun.* **2014**, *5*, 3928.
(50) Dodge, F. A.; Frankenhaeuser, B. Membrane Currents in Isolated Frog Nerve Fibre under Voltage Clamp Conditions. *J. Physiol.* **1958**, *143*, 76.
(51) Mou, Z. X.; Triantis, I. F.; Woods, V. M.; Toumazou, C.; Nikolic, K. A Simulation Study of the Combined Thermoelectric Extracellular Stimulation of the Sciatic Nerve of the Xenopus Laevis: The Localized Transient Heat Block. *IEEE Trans. Biomed. Eng.* **2012**, *59*, 1758−1769.
(52) Korley, J. N.; Yazdi, S.; McHugh, K.; Kirk, J.; Anderson, J.; Putnam, D. One-step Synthesis, Biodegradation and Biocompatibility of Polyesters based on the Metabolic Synthon, Dihydroxyacetone. *Biomaterials* **2016**, *98*, 41−52.
(53) Higa, K.; Kitamura, N.; Kurokawa, T.; Goto, K.; Wada, S.; Nonoyama, T.; Kanaya, F.; Sugahara, K.; Gong, J. P.; Yasuda, K. Fundamental Biomaterial Properties of Tough Glycosaminoglycan Containing Double Network Hydrogels Newly Developed Using the Molecular Stent Method. *Acta Biomater.* **2016**, *43*, 38−49.

DOI: 10.1021/acsami.7b12854
ACS Appl. Mater. Interfaces 2017, 9, 38323−38335